

Oleg V. Surov\* , Marina I. Voronova 

*G.A. Krestov Institute of Solution Chemistry of the Russian Academy of Sciences, Ivanovo, Russia*  
(\*Corresponding author's e-mail: [ovs@isc-ras.ru](mailto:ovs@isc-ras.ru))

## Obtaining Cellulose Nanocrystals in a Medium of Primary Monohydric Alcohols

The lack of a universal method for isolating cellulose nanocrystals (CNCs) has encouraged researchers to look for new methods and approaches as alternatives to traditional sulfuric acid hydrolysis. Acid alcoholysis has long been actively used in cellulose depolymerization processes to obtain a variety of alkyl glycosides and further alcoholysis products. In the present article, the authors continue their earlier research on the synthesis of CNCs in the presence of a sulfuric acid catalyst in an alcoholic environment. In this work, CNCs were obtained from sulfate-bleached pulp in a medium of primary monohydric alcohols ( $C_nH_{2n+1}OH$ ,  $n = 5-8$ ). A maximum CNC yield of 60 % was achieved with pentanol-1 at a sulfuric acid concentration of 50 %. The work revealed that the alcohols studied can be ranked in descending order based on both the acid concentration corresponding to the maximum CNC yield and the yield itself, as follows: pentanol-1, hexanol-1, heptanol-1, and octanol-1. For octanol-1 the maximum CNC yield was 20 % at an acid concentration of 40 %. The physicochemical properties of the isolated CNCs were studied. No surface alkylation of the synthesized CNCs was found to occur during cellulose treatment in the media of the alcohols studied, as the properties of the CNCs, in general, were similar to those of CNCs obtained by standard sulfuric acid hydrolysis. This study broadens the scope of alternative methods to traditional sulfuric acid hydrolysis, and is likely to appeal to researchers engaged in developing novel approaches for CNC extraction.

**Keywords:** cellulose, alcohols, cellulose nanocrystals, synthesis, hydrolysis, alcoholysis, yield, properties.

### Introduction

Cellulose is the most accessible renewable natural resource. As a low-cost biopolymer, cellulose plays an important role in the production of environmentally friendly biocompatible and biodegradable functional materials [1]. Almost defect-free crystalline rod-shaped particles of nanocrystalline cellulose, i.e., cellulose nanocrystals (CNCs), can be isolated from cellulose fibres by acid or enzymatic hydrolysis [2]. Currently, CNCs are of great interest to materials scientists due to their unique combination of physical and chemical properties, including biocompatibility, biodegradability, large specific surface area and high elastic modulus [3]. The scope of CNC application is extensive. CNCs can be used to produce thermal insulation materials, create selective membranes, and deliver systems for medicinal and biologically active compounds. These new materials offer vast opportunities for scientific research and practical applications [4–6].

One of the obstacles to the commercialization of promising materials based on CNCs is that CNC isolation is a rather costly process (associated with the high consumption of energy and reagents, problems with equipment corrosion, environmental risks, and low final product yield). The lack of a universal method for obtaining CNCs has encouraged researchers to search for new methods and approaches (using metal salts, heteropolyacids, ionic liquids, and deep eutectic solvents), as well as to exploit a variety of physical and combined effects (ultrasound, steam explosion, electron beam, supercritical conditions, plasma chemistry, etc.) [7, 8].

The classical method of CNC production is sulfuric acid hydrolysis of cellulose under controlled conditions [9]. Treatment with an acid causes selective hydrolysis of the amorphous regions of cellulose, whereas the presence of glycosidic bonds between the elementary units of cellulose macromolecule is responsible for the relatively low resistance of cellulose to aqueous acid solutions. The generally recognized mechanism of acid hydrolysis of cellulose involves protonation of glycosidic oxygen, followed by cleavage of the glycosidic bond and addition of water molecules [10, 11]. The glycosidic bond cleavage of a cellulose macromolecule in the presence of mineral acids can also be carried out in nonaqueous media. The best studied process from this point of view is alcoholysis, which is the action of solutions of mineral acids in alcohols on the process of cellulose depolymerization [12–14]. Cellulose alcoholysis is similar to hydrolysis, however, the cleavage of glycosidic bonds is accompanied by the acetalization of the resulting free hydroxyl group

[15]. In contrast to complete cellulose hydrolysis, complete alcoholysis produces an alkyl glycoside rather than glucose. It is considered proven that alcoholysis is more effective than hydrolysis and proceeds at a much higher rate, although researchers explain this fact in different ways, and there is no single point of view on this issue [16–19]. However, an analysis of the literature data allows us to conclude that the activation energy for glycosidic bond cleavage during cellulose depolymerization in alcoholic media is lower than that in an aqueous medium, which is responsible for the higher efficiency of cellulose alcoholysis compared to hydrolysis [20]. Currently, cellulose alcoholysis in the presence of an acid catalyst is being actively studied to obtain alkyl glycosides as well as products of further alcoholysis [21–27].

Consequently, it is reasonable to assume that an alcohol medium can be used to obtain CNCs. In one of the recent works [28], we confirmed this hypothesis and showed that cellulose treatment with sulfuric acid in a medium of primary monohydric alcohols makes it possible to obtain CNCs in a higher yield and under milder conditions (at a reduced acid concentration) than hydrolysis in water. We obtained CNCs through sulfuric acid treatment of sulfate-bleached pulp in methanol, ethanol, propanol, and butanol-1 and studied their physicochemical properties. The alcohol media were shown to increase the yield of CNCs and reduce the optimal acid concentration. The properties of the CNCs obtained in the alcohols studied were similar to those of the CNCs obtained by hydrolysis in water, i.e., no functionalization of the surface of the CNC particles with the alkyl groups of the respective alcohols was observed. However, there was an increase in the content of surface sulfate groups and in the surface charge. Under certain synthesis conditions (0.025 g mL<sup>-1</sup> concentration of the pulp suspension, 55 % H<sub>2</sub>SO<sub>4</sub> concentration, 50 °C temperature, 2-hour duration), the use of butanol-1 medium enables us to obtain a maximum possible CNC yield of 60 %.

In this work, we continued to investigate acid cellulose treatment for obtaining CNCs, expanding the range of alcohols used. Namely, in this work, we studied the optimal conditions for CNC synthesis in the media of pentanol-1, hexanol-1, heptanol-1, and octanol-1 and explored the properties of the synthesized CNCs.

### Experimental

To obtain CNCs, dried sulfate-bleached pulp of coniferous wood (State Standard 9571-89, Arkhangelsk Pulp and Paper Mill, Russia) (Table 1), sulfuric acid (98 %, chemically pure, State Standard 4204-77, Chimmed, Russia), pentanol-1 (Chimmed, Russia), hexanol-1, heptanol-1, and octanol-1 (Sigma–Aldrich, USA) were used. All the alcohols used were chemically pure or extra pure and were used without further purification.

Table 1

**Chemical composition of the sulfate-bleached pulp of coniferous wood (State Standard 9571-89)**

Component	Content, %
Cellulose	93–96
Hemicellulose	3–6
Lignin	0.1–0.4
Oils, resins, waxes	0.1–0.2
Ash	0.1–0.15

The process of preparing CNCs was similar to the procedure described earlier [28]. In brief, the pulp ground in a blender was subjected to treatment in sulfuric acid solutions of various concentrations (20–55 wt%) in an appropriate alcohol at 50 °C for 2 hours with vigorous stirring. The concentration of the pulp suspension was 0.025 g mL<sup>-1</sup>. The reaction was carried out in a water bath using a flask equipped with a reflux condenser. After completing the treatment, the heating was stopped, and the reaction mixture was diluted 10-fold with ice-cold deionized water. The CNC suspension was left to settle overnight, followed by decantation of the supernatant. The suspension was then washed in successive cycles of centrifugation (3–5 times for 10 minutes at 8000 rpm) and removal of the supernatant, first with distilled water and then with the appropriate alcohol. The final washing step involved treatment with water. Subsequently, the CNC aqueous suspension was treated with ultrasound (Sonorex DT100, Bandelin, Germany) for 15–30 min, followed by purification with ion exchange resin (TOKEM MB-50(R)) and a dialysis membrane (cut-off of 14 kDa, Roth, Germany) until a constant pH was reached.

The CNC yield was determined by the gravimetric method described elsewhere [29]. The CNC aqueous suspension was left to stand at a temperature of 4 °C for one month, during which large particle aggregates

with a small surface charge precipitated. The CNC suspension was separated from the sediment, and its volume was determined. Three parallel samples of a precisely measured volume were taken, poured into pre-weighed Petri dishes and air-dried until the weight was constant. Having thus determined the concentration of the suspension and knowing its volume, the total yield of the CNCs was calculated taking into account the initial pulp mass (under the assumption that all the water-soluble products had been removed at the stage of washing and dialysis). The relative error in determining the CNC yield in the three parallel samples did not exceed 3 %.

For some further recordings, CNC film samples were obtained by free evaporation of water at room temperature from aqueous CNC suspensions at a concentration of 10 gL<sup>-1</sup>.

A JEOL JEM-1011 transmission electron microscope (TEM) (Japan) with an 8.5 megapixel ORIUS SC1000 W digital camera, an acceleration voltage up to 100 kV, and an image resolution up to 0.3 nm was used to examine the shape and size of the CNC particles. A diluted CNC suspension (approximately 0.01 gL<sup>-1</sup>) was sonicated and then coated onto a copper TEM grid with a 200-mesh size. After complete drying, the samples were treated by shadowing with tungsten oxide WO<sub>3</sub> on a JEOL JEE-4C vacuum evaporator.

The elemental composition of the CNC films was determined by X-ray energy dispersive analysis using an X-Max 6 spectrometer (Oxford Instruments NanoAnalysis) with an x-ACT detector included in a VEGA 3 TESCAN scanning electron microscope (SEM). Range of the analyzed elements: <sub>4</sub>Be–<sub>94</sub>Pu. The equipment was synchronized with the SEM electron gun, allowing detailed surface elemental mapping and providing a highly accurate analysis.

The FTIR spectra were obtained on a VERTEX 80v spectrophotometer (Bruker, Germany) in the frequency range of 4000–400 cm<sup>-1</sup>. The samples were pressed into tablets containing 1 mg of the analyte and 100 mg of potassium bromide.

The Raman spectra of the CNC samples were recorded on a Confotec NR 500 instrument (Sol Instruments, Belarus). The spectral range for recording the Raman signals ranged from 30 cm<sup>-1</sup> to approximately 6000 cm<sup>-1</sup> and a spectral resolution of 0.25 cm<sup>-1</sup> was achieved by simultaneous use of 3 lasers (785 nm, 633 nm, 488 nm) through automatic switching of the necessary components within the system.

The sizes of the CNC particles in the aqueous suspensions were measured by the dynamic light scattering method (DLS) (emission wavelength of 633 nm) on a Zetasizer Nano ZS device (Malvern Instruments Ltd., UK) operating in the range of 0.3 nm – 6 μm. The measurements were carried out in disposable polystyrene cuvettes at a 0.1 gL<sup>-1</sup> suspension concentration. During the measurements, the cuvette with the test sample was thermostated at a temperature of 20 °C. The obtained particle size values are the results of averaging over five successive measurement cycles. The value obtained in each cycle is, in turn, the result of automatic processing of 10–15 measurements. The sizes of the CNC particles obtained by the DLS method are averaged values for the hydrodynamic diameters of equivalent spheres and do not reflect the real physical sizes of anisotropic rod-shaped CNC particles; rather, they are used for comparative analysis [30].

The surface charge of the CNC particles in an aqueous suspension was evaluated by the ζ-potential (Zetasizer Nano ZS). The obtained ζ-potential values were the results of averaging over five successive measurement cycles.

X-ray diffraction (XRD) analysis was carried out on a Bruker D8 Advance diffractometer according to the Bragg-Brentano scheme using Cu-K<sub>α</sub> radiation (λ = 0.1542 nm). The angular scanning range was 2–45° with a 0.01° step. A Vantec-1 high-speed meter was used. The pulse acquisition time at each scanning point was 0.5 s. The CNC crystallinity index according to Segal [31] was determined as

$$IC = (I_{200} - I_a)/I_{200},$$

where  $I_{200}$  is the intensity of the reflection corresponding to the crystallographic plane (200) and  $I_a$  is the intensity of the amorphous halo (the minimum between the peaks corresponding to crystallographic planes (200) and (110)).

The sizes of the CNC crystallites ( $L$ ) were calculated using the Scherrer formula [32]:

$$L = 0.9\lambda/\beta\cos\theta,$$

where  $\lambda$  is the X-ray wavelength, nm;  $\beta$  is the full width of the diffraction peak, measured at its half-maximum, rad.;  $\theta$  is the diffraction angle of the peak, degrees.

Thermogravimetric analysis was performed on a TG 209 F1 Iris thermomicrobalance (Netzsch, Germany) using platinum crucibles in an atmosphere of dry argon at a flow rate of 30 ml min<sup>-1</sup> and a heating rate of 10 K min<sup>-1</sup>.

The degree of polymerization of the CNC samples was determined by the viscosity of the solutions in cadoxene, as described earlier [33].

### Results and Discussion

Pulp treatment was carried out at a temperature of 50 °C for two hours with intense stirring, changing sulfuric acid concentration (from 20 to 55 wt%). Figure 1 shows the CNC yield in the media of alcohols studied: pentanol-1, hexanol-1, heptanol-1, and octanol-1. Each of the alcohols is characterized by its own sulfuric acid concentration range in which CNCs can be isolated. This range is limited by the minimum sulfuric acid concentration, at which virtually no depolymerization of cellulose occurs (the CNC yield is low), or the maximum concentration, at which cellulose is depolymerized to low-molecular-weight oligomers, glucose and other soluble products (the CNC yield is also low). The maximum CNC yield and the proper optimal acid concentration depend on the alcohol used. Both the acid concentration corresponding to the maximum CNC yield and the yield itself decreased in the pentanol-1, hexanol-1, heptanol-1, and octanol-1 series (Table 2).

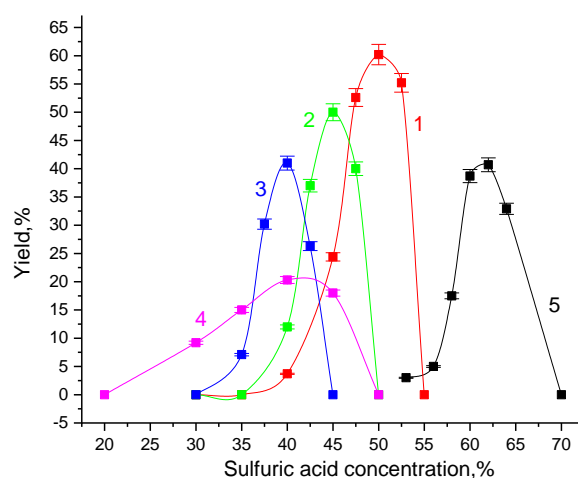


Figure 1. CNC yield during pulp treatment in pentanol-1 (1), hexanol-1 (2), heptanol-1 (3), and octanol-1 (4). For comparison, the curve for hydrolysis in water is shown (5) [28]

Table 2

**The concentration of sulfuric acid corresponding to the maximum CNC yield in the alcohols studied. For comparison, data for hydrolysis in water is shown [28]**

Medium	H <sub>2</sub> SO <sub>4</sub> concentration range for CNC isolation, wt%	H <sub>2</sub> SO <sub>4</sub> concentration corresponding to the maximum CNC yield, wt%	Maximum CNC yield, %
Pentanol-1	35–55	50	60±2
Hexanol-1	35–50	45	45±1
Heptanol-1	30–45	40	23±1
Octanol-1	20–50	40	20±1
Water	53–70	62	41±1

It should be taken into account that a certain amount of acid is spent on interactions with alcohols to form the respective alkyl sulfates and dialkyl ethers [10, 20]. As a result of interactions with sulfuric acid, alcohols become darker, from light yellow for pentanol-1 to dark brown for octanol-1. Titration of the reaction medium with sodium hydroxide after alcoholysis was completed showed that the sulfuric acid consumption in esterification reactions was approximately 30 % of the initial acid amount (determined for the sulfuric acid–alcohol systems, in which the maximum CNC yield was registered). For this reason, the acid concentrations in Table 2 and Figure 1 are somewhat overestimated because the initial concentrations are given without considering acid consumption for interactions with alcohols.

The transmission electron microscopy (TEM) images show that the CNC particles have an anisotropic rod-like shape (Fig. 2). The length of the particles ranges from approximately 200 to 400 nm, and the diame-

ter is approximately 10–20 nm, although aggregates of the particles formed due to their lateral interaction are observed.

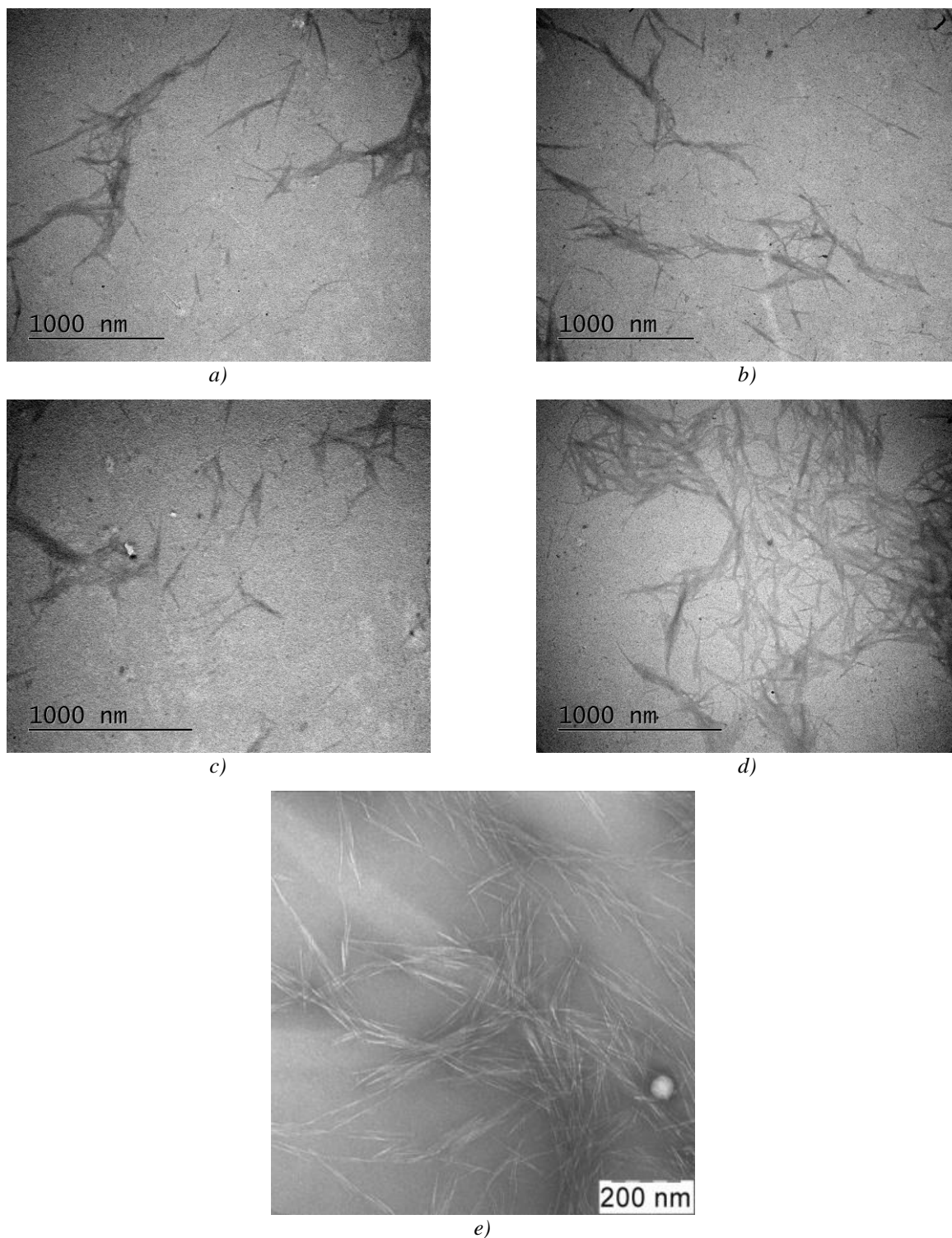


Figure 2. TEM images of CNC particles obtained in pentanol-1 (*a*), hexanol-1 (*b*), heptanol-1 (*c*), and octanol-1 (*d*). For comparison, an image of CNC particles obtained through hydrolysis in water is shown (*e*) [28]. The scales are 1  $\mu\text{m}$  (*a–d*), and 200 nm (*e*)

The data obtained by DLS were in good agreement with the TEM images of the CNC particles. The DLS experimental data (Fig. 3) for aqueous suspensions show polydispersity of the size distribution of the CNC particles. Two groups of particles can be distinguished at approximately 100–300 and 10–40 nm in size.

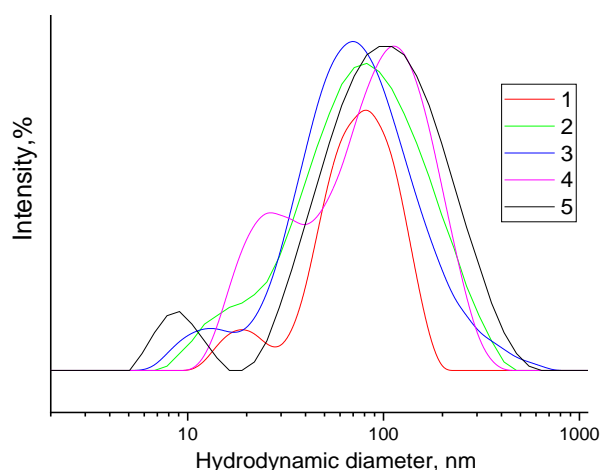


Figure 3. Hydrodynamic diameters of the CNC particles obtained in pentanol-1 (1), hexanol-1 (2), heptanol-1 (3), and octanol-1 (4). For comparison, data for CNC particles obtained through hydrolysis in water are shown (5) [28]

Notably, the results shown in Figures 2 and 3 and further discussed in the article refer to the CNCs obtained with the maximum yield.

Aqueous suspensions of CNCs exhibit high colloidal stability for a long time (a month or longer), which is due to the significant charge of sulfate groups grafted onto the surface of the CNC particles during sulfuric acid treatment. The  $\zeta$ -potential values of the aqueous CNC suspensions and the sulfur content (as part of the surface sulfate groups) of the samples are given in Table 3.

Table 3

**Particle charge and elemental composition of the CNC samples obtained in the alcohols studied. For comparison, the data for hydrolysis in water are shown [28]**

Medium	$\zeta$ -potential, mV	*Elemental composition, %			O/C ratio
		S	C	O	
Pentanol-1	-47±3	1.2±0.1	54.5±0.1	45.9±0.1	0.84
Hexanol-1	-46±3	1.0±0.1	54.1±0.1	44.9±0.1	0.83
Heptanol-1	-45±2	0.9±0.1	52.9±0.1	45.5±0.1	0.86
Octanol-1	-41±2	0.8±0.1	53.5±0.1	46.6±0.1	0.87
Water	-38±2	0.7±0.1	47.6±0.1	39.6±0.1	0.83

\* Determined by X-ray energy dispersive analysis

The oxygen-to-carbon ratios for all the CNC samples are close to the theoretical value of 0.83 for a pure cellulose surface [34, 35].

The thermal stability of CNCs largely depends on the content of surface sulfate groups. The sulfate groups catalyze the thermal decomposition of CNC samples, decreasing their thermal stability [36]. The high sulfur content in the samples is confirmed by the lower decomposition temperatures than those of CNCs with surface carboxyl groups or microcrystalline cellulose (MCC) [37]. The TG curves of the CNC samples under study are characterized by three main mass loss regions (Fig. 4). The first region (approximately 100 °C) is associated with water evaporation, the second region (from approximately 200 to 400 °C) is associated with CNC pyrolysis and the formation of gaseous products, and the third region (above 400 °C) is associated with the thermal decomposition of carbonaceous matter [38].

The X-ray diffraction patterns of the CNC films shown in Figure 5 indicate that the resulting CNCs are cellulose I. Despite the relatively low intensity of the diffraction patterns, there is a clearly visible peak at a Bragg angle of  $2\theta = 22.9^\circ$ , an implicit double peak in the region  $2\theta = 15-17^\circ$ , and a diffraction peak of low intensity at approximately  $2\theta = 34.5^\circ$ , which corresponds to the crystallographic planes (200), (1-10), (110), and (004) of cellulose I $\beta$ , respectively [39]. The CNC films are characterized by a high crystallinity index (approximately 90 %) and a crystallite size of approximately 4 nm (perpendicular to the (200) crystallographic plane) (Table 4).

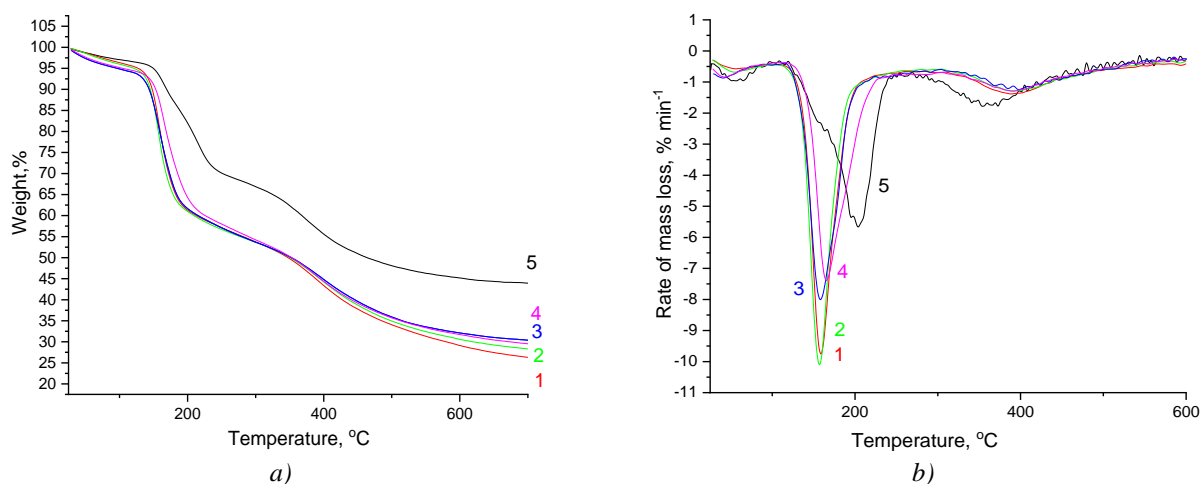


Figure 4. TG (a) and DTG (b) curves of the CNC samples obtained in pentanol-1 (1), hexanol-1 (2), heptanol-1 (3), and octanol-1 (4). For comparison, curves for the CNC sample obtained by hydrolysis in water (5) [28] are shown

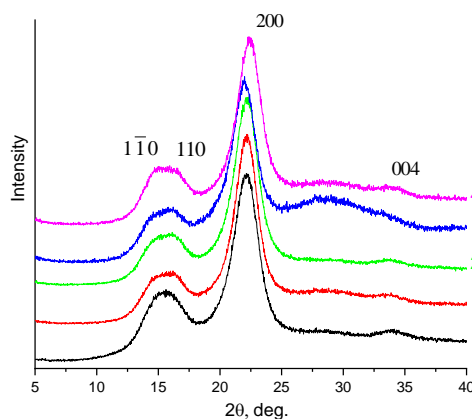


Figure 5. X-ray diffraction patterns for CNC films obtained in pentanol-1 (1), hexanol-1 (2), heptanol-1 (3), and octanol-1 (4). For comparison, diffraction patterns for the CNC sample obtained by hydrolysis in water (5) [28] are shown

Table 4

**Properties of the CNC samples obtained in the alcohols studied and in water [28]**

Medium	Crystallinity index, %	Crystallite size perpendicular to the (200) plane, nm
Pentanol-1	87±4	3.9±0.2
Hexanol-1	86±4	4.1±0.2
Heptanol-1	84±4	3.6±0.1
Octanol-1	86±4	4.0±0.2
Water	80±4	3.3±0.1

The degree of polymerization of the CNC samples ranges from approximately 90 to 110, which is characteristic of the leveling off degree of polymerization of nanocrystalline cellulose; i.e., CNCs were formed, and the crystallites were left intact [40, 41].

Figure 6 shows the FTIR spectra of the CNC samples obtained in pentanol-1, hexanol-1, heptanol-1, and octanol-1. The spectra are typical of cellulose and are characterized by intense absorption bands in the wavenumber regions of 3500–3300 cm<sup>-1</sup> and 3000–2750 cm<sup>-1</sup>, which correspond to the stretching vibrations of the OH and C–H bonds of the cellulose macromolecule. In the range of 1500–1200 cm<sup>-1</sup>, bending vibra-

tions of the OH, CH and CH<sub>2</sub> groups appear. The absorption region at 1200–950 cm<sup>-1</sup> refers to the stretching vibrations of the C–O and C–C bonds of the pyranose ring. The bands in the frequency range of 950–400 cm<sup>-1</sup> are caused by the vibrations of large fragments of the cellulose macromolecule, as well as out-of-plane vibrations of the hydroxyl groups. The fairly intense band at approximately 1640 cm<sup>-1</sup> is due to the stretching vibrations of the adsorbed water. In general, the FTIR spectra of the CNC samples obtained in the alcohols studied are identical to those obtained by standard sulfuric acid hydrolysis [28].

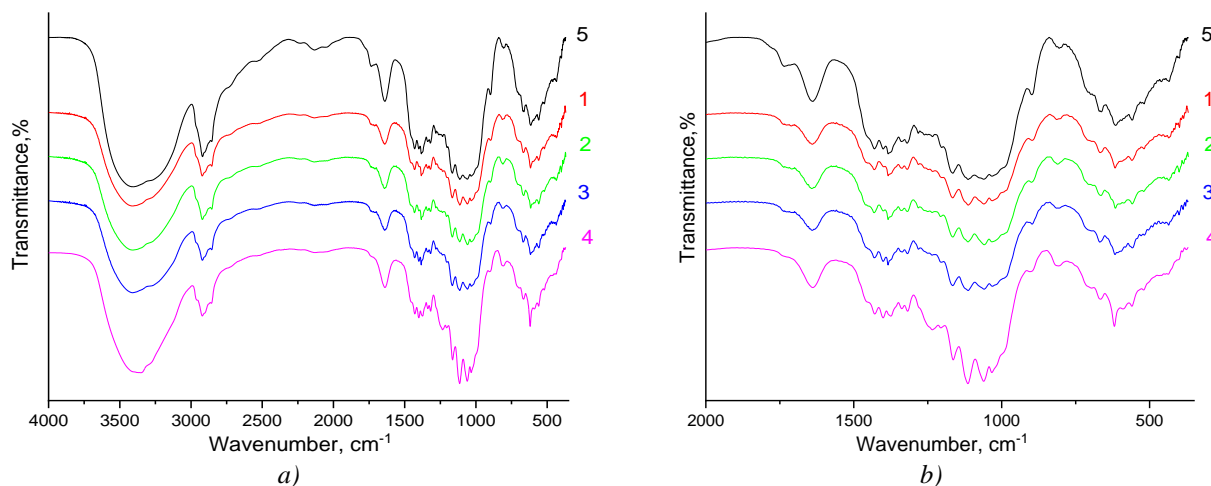


Figure 6. FTIR spectra of the CNC samples obtained in pentanol-1 (1), hexanol-1 (2), heptanol-1 (3), and octanol-1 (4) in the wavenumber ranges of 4000–400 cm<sup>-1</sup> (a) and 2000–400 cm<sup>-1</sup> (b). For comparison, the FTIR spectrum of the CNC sample obtained by hydrolysis in water (5) [28] is shown

The Raman spectra of the studied CNC samples generally correspond to MCC spectra [42]. The intense peak at a frequency of 1096 cm<sup>-1</sup> is attributed to the stretching vibrations of the C–O and C–C bonds of the pyranose ring (Fig. 7). The intense peak at 1380 cm<sup>-1</sup> in the “fingerprint” region characterizes the ring bending vibrations. The intense bands in the spectral regions of 2800–3000 cm<sup>-1</sup> and 1430–1480 cm<sup>-1</sup> describe the stretching and bending vibrations of the CH groups, respectively. The less intense band in the range of 3100–3600 cm<sup>-1</sup> is ascribed to the stretching vibrations of the OH groups [43, 44].

The CNCs samples obtained in the alcohols studied were cellulose I, as evidenced by the presence of the characteristic peak at 1480 cm<sup>-1</sup> (CH<sub>2</sub> bending vibrations of the hydroxymethyl group in the *tg* conformation) and 380 cm<sup>-1</sup> (out-of-plane vibrations of the pyranose ring). In addition, the high intensity of the peak at 380 cm<sup>-1</sup> proves the high crystallinity of the samples [43]. Another peak at 93 cm<sup>-1</sup> (twisting deformations along the polymer chain), also used to characterize the crystallinity of cellulose samples [45, 46], has a lower intensity and is much less pronounced.

In the spectra of the CNC samples under study, the bands at 1060 and 1274 cm<sup>-1</sup> are attributed to the symmetric and asymmetric O=S=O stretching vibrations of sulfate esters, respectively [47]. For the CNCs under study, there are surface sulfate groups on the surface of the nanoparticles as a result of esterification of the hydroxyl groups (mainly the primary hydroxyl groups at the carbon atom C6). The intensity and width of the bands at 1060 and 1274 cm<sup>-1</sup> increase as the substitution degree increases, i.e., as the content of the surface sulfate groups increases. The sulfate groups grafted onto the surface of the CNC particles also affect the vibrational modes of the entire pyranose. Therefore, for the CNC samples under study, the ratio of the intensities of the bands at 2896 and 2969 cm<sup>-1</sup> changes (these bands reflect the CH and CH<sub>2</sub> stretching vibrations, respectively). The intensity of the CH<sub>2</sub> stretching vibrations increases when going from octanol-1 to pentanol-1, and that of the CH vibrations decreases. In comparison, for the CNC sample obtained by hydrolysis in water, the peak at 2896 cm<sup>-1</sup> (CH vibrations) is much greater than that of the other materials, and the band at 2969 cm<sup>-1</sup> (CH<sub>2</sub> vibrations) appears only as a shoulder. However, the replacement of protons with sulfate groups as a result of esterification does not reduce the intensity of the bands in the range of 3100–3600 cm<sup>-1</sup> (stretching vibrations of the OH groups) compared to that of MCC [42] since the substitution degree is low.

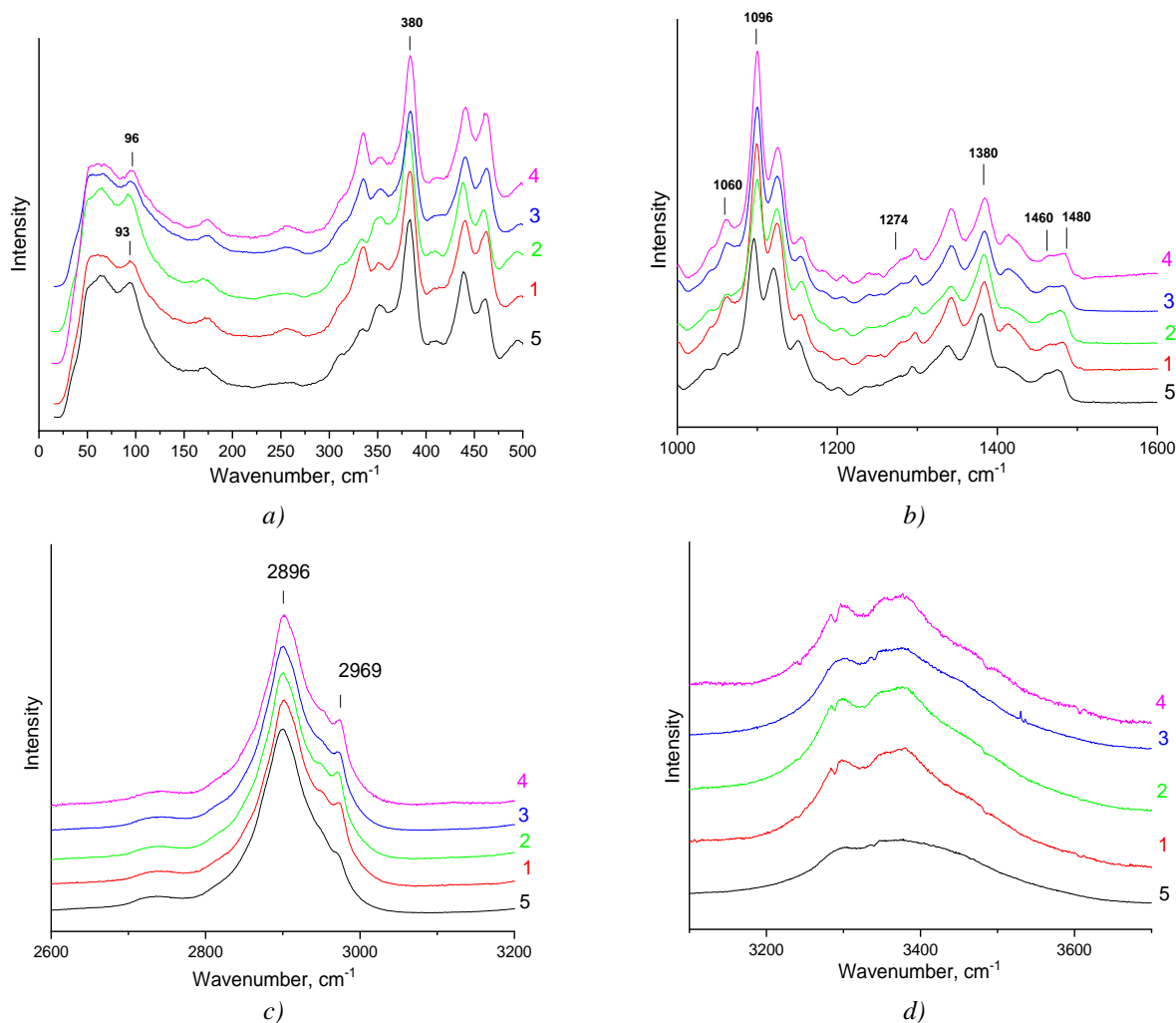


Figure 7. Raman spectra of the CNC samples obtained in pentanol-1 (4), hexanol-1 (3), heptanol-1 (2), octanol-1 (1), and by hydrolysis in water (5) [28] in the wavenumber ranges of 0–500  $\text{cm}^{-1}$  (a), 1000–1600  $\text{cm}^{-1}$  (b), 2600–3200  $\text{cm}^{-1}$  (c), and 3100–3700  $\text{cm}^{-1}$  (d), respectively. The spectra are normalized to the band at 1096  $\text{cm}^{-1}$

The formation of ester bonds at C6 may be responsible for the appearance of rotamers of the unsubstituted surface  $\text{CH}_2\text{OH}$  groups, while in the crystalline phase, they are in the *tg* conformation (for cellulose I $\alpha$  and I $\beta$ ) [43, 48, 49]. The intensity ratio of the bands at 1460 and 1480  $\text{cm}^{-1}$  is used to estimate the *gt/tg* rotamer ratio of the  $\text{CH}_2\text{OH}$  group of cellulose I [50]. The higher intensity of the band at 1460  $\text{cm}^{-1}$  for the CNC samples obtained in the alcohols studied indicates an increase in the proportion of rotamers of the  $\text{CH}_2\text{OH}$  groups with the *gt* conformation.

As we have previously shown [28], an acid treatment of cellulose in methanol, ethanol, propanol, and butanol-1 is not accompanied by CNC surface alkylation. We observed the same phenomenon during CNC isolation in pentanol-1, hexanol-1, heptanol-1, and octanol-1. The elemental analysis, FTIR and Raman spectra did not reveal any differences between the CNC samples obtained in the alcohols studied and the CNC sample obtained by hydrolysis in water (Table 3, Figures 6, 7) [28].

When the surface of CNC particles are alkylated during alcoholysis, one expects an increase in the intensity of the absorption bands of the methylene groups and the appearance of new bands corresponding to the methyl groups. In this case, symmetric and asymmetric stretching vibrations, as well as bending vibrations of the C–H bond, are expected to appear in the FTIR spectra in the wavenumber ranges of 2800–3000  $\text{cm}^{-1}$ , 1365–1395  $\text{cm}^{-1}$ , and 1430–1470  $\text{cm}^{-1}$ , respectively. We did not observe any changes in the Raman spectra associated with possible alkylation of the surface of the CNC particles during alcoholysis either. In the case of CNC alkylation, one expects an increase in the intensity of the bands in the Raman spectra associated with the stretching and bending vibrations of the methyl and methylene groups (spectral regions of 2800–3000  $\text{cm}^{-1}$  and 1430–1480  $\text{cm}^{-1}$ , respectively).

Apparently, in contrast to the homogeneous process of alkylation of glucose during complete alcoholysis, the heterogeneous process of acid cellulose treatment in alcohol media during CNC production does not involve CNC surface alkylation. One possible cause of this difference may be that, despite the use of an alcohol medium, hydrolysis ultimately occurs due to the presence of water in the alcohol, the acid catalyst, and/or cellulose. Alternatively, water can result from side reactions of alcohol esterification (part of the sulfuric acid will be irretrievably consumed by the reactions) [51].

We have previously shown [28] that in the series water–methanol–ethanol–propanol–butanol-1, the acid concentration corresponding to the maximum yield of CNCs decreases, and the yield itself increases. Since protonation of the glycosidic oxygen in an aqueous environment with subsequent cleavage of the glycosidic bond in the elementary units of the cellulose macromolecule requires rather harsh conditions (strong acid, high proton concentration), we hypothesized that the process of cellulose depolymerization can proceed more efficiently in an environment in which the solvated proton has much greater acidity than that of the hydronium ion  $\text{H}_3\text{O}^+$  (pKa  $-1.7$ ). Protic solvents, particularly alcohols, can create such an environment. According to the literature, the pKa values for protonated alcohols decrease in the series  $\text{CH}_3\text{OH}_2^+$ ,  $\text{C}_2\text{H}_5\text{OH}_2^+$ ,  $(\text{CH}_3)_2\text{CHOH}_2^+$ , and  $(\text{CH}_3)_3\text{COH}_2^+$  and are, respectively,  $-2.2$ ,  $-2.4$ ,  $-3.2$ , and  $-3.8$  [52, 53].

We found [28] that the dependence of the maximum yield of CNCs on the pKa value of the protonated solvent (water and alcohols, methanol, ethanol, propanol, and butanol-1) is well described by the following quadratic function:  $\text{Max.yield} = a \cdot \text{pKa}^2 + b \cdot \text{pKa} + c$ , where Max.yield is the maximum yield of the CNCs; pKa are the pKa values of the protonated solvents (water, methanol, ethanol, propanol, and butanol-1); and  $a$ ,  $b$ , and  $c$  are constants. Notably, we used published data on the pKa values for protonated isopropanol  $(\text{CH}_3)_2\text{CHOH}_2^+$  and tert-butanol  $(\text{CH}_3)_3\text{COH}_2^+$ , although the experiment was carried out with propanol and butanol-1.

The coordinates of the parabola vertex, according to the parameters of this quadratic equation are  $\text{pKa} = -3.65$  and  $\text{Max.yield} = 60.08$ . This means that under the given conditions for CNC synthesis (the pulp suspension concentration of  $0.025 \text{ g ml}^{-1}$ , a temperature of  $50 \text{ }^\circ\text{C}$ , and a duration of 2 hours), the butanol-1 medium enables us to obtain a maximum possible CNC yield of approximately 60 %. In this regard, it would be interesting to check whether the values of the maximum CNC yield obtained in the media of pentanol-1, hexanol-1, heptanol-1, or octanol-1 lie on the descending branch of the parabola. It is difficult to answer this question because the pKa values for the protonated alcohols, pentanol-1, hexanol-1, heptanol-1, and octanol-1, are, to our knowledge, unavailable in the literature.

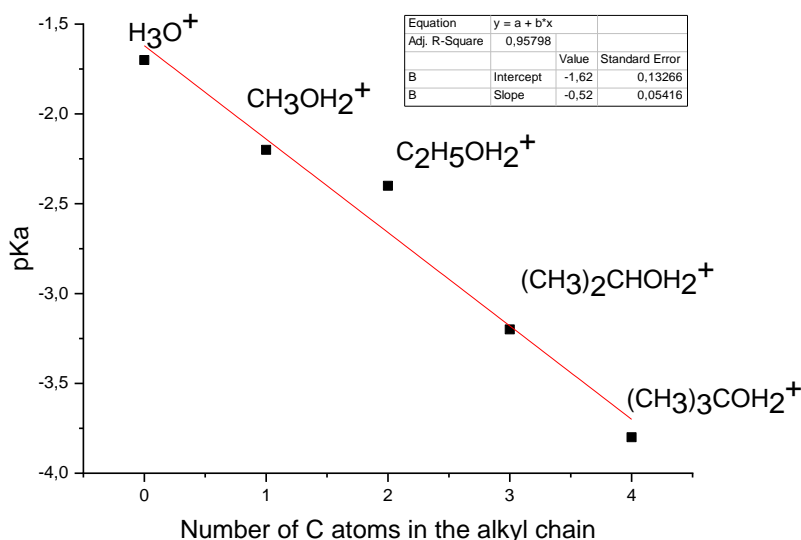


Figure 8. Dependence of the pKa of a protonated solvent (water, methanol, ethanol, isopropanol, or tert-butanol) on the number of carbon atoms in the alkyl chain

However, since, in the series  $\text{H}_3\text{O}^+ - \text{CH}_3\text{OH}_2^+ - \text{C}_2\text{H}_5\text{OH}_2^+ - (\text{CH}_3)_2\text{CHOH}_2^+ - (\text{CH}_3)_3\text{COH}_2^+$ , the dependence of the pKa values on the alkyl chain length is well approximated by a linear function (Figure 8 and the inset in it), it is possible to estimate the probable pKa values for protonated pentanol-1, hexanol-1, heptanol-1, and octanol-1. According to the parameters of the linear equation given in the inset in Figure 8, these val-

ues are  $-4.2 \pm 0.4$ ,  $-4.7 \pm 0.5$ ,  $-5.3 \pm 0.6$  and  $-5.8 \pm 0.6$  for protonated pentanol-1, hexanol-1, heptanol-1, and octanol-1, respectively.

Thus, based on the estimated pKa values for protonated pentanol-1, hexanol-1, heptanol-1, and octanol-1, plotting the dependence of the maximum yield of the synthesized CNCs on the pKa of the protonated alcohols from methanol to octanol-1 is possible (Fig. 9).

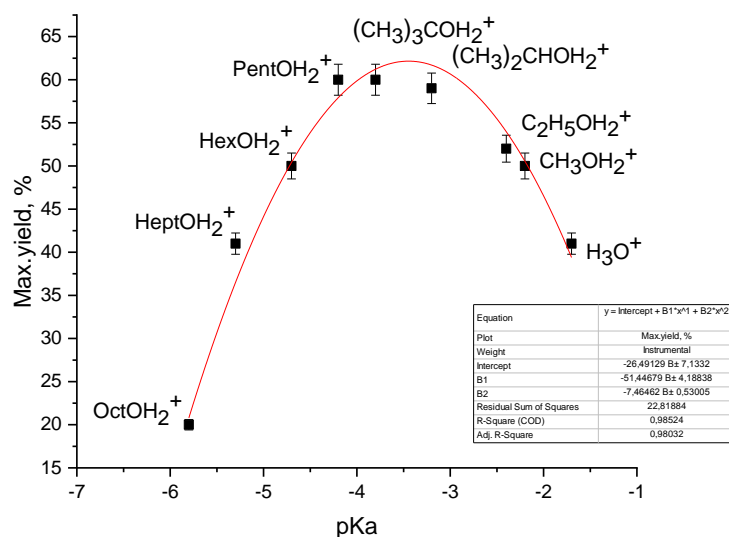


Figure 9. Dependence of the maximum CNC yield on the pKa values of protonated solvents (water and alcohols)

Figure 9 indeed shows that the values of the maximum CNC yield obtained in the media of pentanol-1, hexanol-1, heptanol-1, and octanol-1 lie on the descending branch of the parabola. In addition, in pentanol-1, a maximum yield of 60 % is achieved at an even lower acid concentration (50 wt%) than that in butanol-1 (55 wt%).

Thus, the dependence of the maximum CNC yield on the pKa of protonated alcohols is extreme and is quite well described by a parabola with a vertex corresponding to the pKa values of protonated butanol-1 and pentanol-1 (approximately  $-4$ ) and a yield of approximately 60 %. The extreme nature of the dependence is apparently determined by the competition of at least two factors. On the one hand, the increase in the acidity of the protonated alcohols with increasing length of the alkyl radical (the increase in the negative pKa values) promoted cellulose depolymerization and, accordingly, an increase in the CNC yield. On the other hand, due to process heterogeneity, the hydrolysis and alcoholysis rates (and, accordingly, cellulose depolymerization) depend on phenomena such as cellulose wetting and swelling, adsorption and diffusion of reagents. The process of cellulose swelling is reduced to the penetration of solvent molecules into the intermolecular space of cellulose and solvation of the respective sections of the polymer chain, which changes the intermolecular interactions between the macromolecules, increases their mobility and makes it easier for the reagents to enter the intermolecular space. However, the swelling degree of cellulose is known to be lower for aliphatic alcohols than for water and decreases with increasing length of the hydrocarbon radical [54]. Therefore, this factor does not increase the hydrolysis rate in an alcohol environment.

In a recently published paper, Zhao et al. [55] studied the mechanism of catalytic conversion of cellulose into 5-ethoxymethylfurfural and ethyl levulinate in ethanol and water-ethanol mixtures. A mixture of Brønsted and Lewis acids ( $\text{H}_2\text{SO}_4$  and  $\text{AlCl}_3$ ) was used to catalyze the reaction. Based on the experimental data and results of computer simulations, the authors showed that the presence of water lowers the energy barrier of the depolymerization of cellobiose (as a model of cellulose) compared to that for pure ethanol. Thus, the presence of water in the system contributes to the maximum conversion of cellulose into products of alcoholysis.

Apparently, when CNCs are produced in an alcohol medium, water plays a key role, and the alcohol medium promotes hydrolysis, increasing the yield of the synthesized CNCs and lowering the optimal acid concentration. Obviously, further research, including computer simulation methods, is required for a detailed elucidation of the mechanism of acid hydrolysis of cellulose in an alcohol environment during CNC synthesis, which is the goal of our further work.

### Conclusions

For the first time, CNCs were obtained by sulfuric acid treatment of sulfate-bleached pulp in pentanol-1, hexanol-1, heptanol-1, and octanol-1, and their physicochemical properties were studied. In pentanol-1, the maximum CNC yield was 60 % at a sulfuric acid concentration of 50 wt%. During cellulose treatment in the alcohol media, no alkylation of the CNC surface occurs, and the properties of the CNCs are similar to those of the CNCs obtained by standard sulfuric acid hydrolysis. In CNC synthesis, water plays a key role, and alcohol media promote hydrolysis, increasing the CNC yield and reducing the optimal acid concentration. Additional studies in organic solvents and mixed aqueous-organic media are necessary to fully elucidate the mechanism of cellulose solvolysis during the production of CNCs.

### Author Information\*

\*The authors' names are presented in the following order: First Name, Middle Name and Last Name

**Oleg Valentinovich Surov** (corresponding author) — Candidate of Chemical Sciences, Senior Researcher, G.A. Krestov Institute of Solution Chemistry of the Russian Academy of Sciences, Akademicheskaya St., 1, 153045, Ivanovo, Russia; e-mail: [ovs@isc-ras.ru](mailto:ovs@isc-ras.ru), <https://www.scopus.com/redirect.uri?url=https://orcid.org/0000-0002-7164-364X&authorId=8338558100&origin=AuthorProfile&orcidId=0000-0002-7164-364X&category=orcidLinkhttps://orcid.org/0000-0002-7164-364X>

**Marina Igorevna Voronova** — Candidate of Chemical Sciences, Senior Researcher, G.A. Krestov Institute of Solution Chemistry of the Russian Academy of Sciences, Akademicheskaya St., 1, 153045, Ivanovo, Russia; e-mail: [miv@isc-ras.ru](mailto:miv@isc-ras.ru), <https://www.scopus.com/redirect.uri?url=https://orcid.org/0000-0002-7164-364X&authorId=8338558100&origin=AuthorProfile&orcidId=0000-0002-7164-364X&category=orcidLinkhttps://www.scopus.com/redirect.uri?url=https://orcid.org/0000-0002-8535-6940&authorId=6701319869&origin=AuthorProfile&orcidId=0000-0002-8535-6940&category=orcidLinkhttps://orcid.org/0000-0002-8535-6940>

### Author Contributions

The manuscript was written through contributions of all authors. All authors have given approval to the final version of the manuscript. **CRedit**: **Oleg Valentinovich Surov** conceptualization, data curation, investigation, methodology, validation, visualization, writing-original draft, writing-review & editing; **Marina Igorevna Voronova** data curation, formal analysis, validation, visualization, writing-review & editing.

### Acknowledgments

Authors thank the *Upper Volga Region Centre of Physicochemical Research* (Ivanovo, Russia) for some measurements taken with the use of its equipment.

### Conflicts of Interest

The authors declare no conflict of interest.

### References

- 1 Habibi, Y., Lucia, L. A., & Rojas, O. J. (2010). Cellulose nanocrystals: Chemistry, self-assembly, and applications. *Chem. Rev.*, *110*(6), 3479–3500. <https://doi.org/10.1021/cr900339w>
- 2 Klemm, D., Kramer, F., Moritz, S., Lindstrom, T., Ankerfors, M., Gray, D., & Dorris, A. (2011). Nanocelluloses: a new family of nature-based materials. *Angew. Chem. Int. Ed.*, *50*(24), 5438–5466. <https://doi.org/10.1002/anie.201001273>
- 3 Moon, R. J., Martini, A., Nairn, J., Simonsen, J., & Youngblood, J. (2011). Cellulose nanomaterials review: Structure, properties and nanocomposites. *Chem. Soc. Rev.*, *40*, 3941–3994. <https://doi.org/10.1039/C0CS00108B>
- 4 Thomas, B., Raj, M. C., Athira, K. B., Rubiyah, M. H., Joy, J., Moores, A., Drisko, G. L., & Sanchez, C. (2018). Nanocellulose, a versatile green platform: From biosources to materials and their applications. *Chem. Rev.*, *118*(24), 11575–11625. <https://doi.org/10.1021/acs.chemrev.7b00627>
- 5 Dhali, K., Ghasemlou, M., Daver, F., Cass, P., & Adhikari, B. (2021). A review of nanocellulose as a new material towards environmental sustainability. *Sci. Total Environ.*, *775*, 145871. <https://doi.org/10.1016/j.scitotenv.2021.145871>

- 6 Zhu, H., Luo, W., Ciesielski, P. N., Fang, Z., Zhu, J. Y., Henriksson, G., Himmel, M. E., & Hu, L. (2016). Wood-derived materials for green electronics, biological devices, and energy applications. *Chem. Rev.*, *116*(16), 9305–9374. <https://doi.org/10.1021/acs.chemrev.6b00225>
- 7 Kargarzadeh, H., Ahmad, I., Thomas, S., & Dufresne, A. (2017). *Handbook of nanocellulose and cellulose nanocomposites* (1st ed.). Wiley.
- 8 Hu, L., Jiang, F., & Chen, C. (2023). *Emerging nanotechnologies in nanocellulose*. Springer International Publishing.
- 9 Rana, A. K., Frollini, E., & Thakur, V. K. (2021). Cellulose nanocrystals: Pretreatments, preparation strategies, and surface functionalization. *Int. J. Biol. Macromol.*, *182*, 1554–1581. <https://doi.org/10.1016/j.ijbiomac.2021.05.119>
- 10 Deng, W., Zhang, H., Xue, L., Zhang, Q., & Wang, Y. (2015). Selective activation of the C–O bonds in lignocellulosic biomass for the efficient production of chemicals. *Chin. J. Catal.*, *36*(9), 1440–1460. [https://doi.org/10.1016/S1872-2067\(15\)60923-8](https://doi.org/10.1016/S1872-2067(15)60923-8)
- 11 Bikales, N. M., & Segal, L. (1971). *Cellulose and cellulose derivatives* (2nd ed., part IV). Wiley.
- 12 Reeves, R. E., Schwartz, W. M., & Giddens, J. E. (1946). The alcoholysis of cellulose. *J. Am. Chem. Soc.*, *68*(7), 1383–1385. <https://doi.org/10.1021/ja01211a505>
- 13 Reeves, R. E., Mazzeno Jr, L. W., & Hoffpauir, C. L. (1950). The heterogeneous methanolysis of native and mercerized cotton cellulose. *J. Am. Chem. Soc.*, *72*(10), 4773–4777. <https://doi.org/10.1021/ja01166a121>
- 14 Yamada, T., Yamaguchi, M., Kubo, S., & Hishikawa, Y. (2015). Direct Production of Alkyl Levulinates from Cellulosic Biomass by a Single-Step Acidic Solvolysis System at Ambient Atmospheric Pressure. *BioResources*, *10*(3). <https://doi.org/10.15376/biores.10.3.4961-4969>
- 15 Rogovin, Z. A. (1972). *Khimiya tsellyulozy [Chemistry of cellulose]*. Khimia [in Russian].
- 16 Valley, R.B. (1955). A study of the alcoholysis of cellulose. *Text. Res. J.*, *25*(11), 930–939. <https://journals.sagepub.com/toc/trjc/25/11> <https://doi.org/10.1177/004051755502501104>
- 17 Heath, J. E., & Jeffries, R. (1968). The alcoholysis of cellulose. *J. Appl. Polym. Sci.*, *12*(3), 455–465. <https://doi.org/10.1002/app.1968.070120306>
- 18 Bouchard, J., Lacelle, S., Chornet, E., Vidal, P. P., & Overend, R. R. (1993). Mechanism of depolymerization of cellulose by ethylene glycol solvolysis. *Holzforschung*, *47*(4), 291–296. <https://doi.org/10.1515/hfsg.1993.47.4.291>
- 19 Zhu, S., Guo, J., Wang, X., Wang, J., & Fan, W. (2017). Alcoholysis: A Promising Technology for Conversion of Lignocellulose and Platform Chemicals. *ChemSusChem*, *10*(12), 2547–2559. Portico. <https://doi.org/10.1002/cssc.201700597>
- 20 Deng, W., Liu, M., Zhang, Q., & Wang, Y. (2011). Direct transformation of cellulose into methyl and ethyl glucosides in methanol and ethanol media catalyzed by heteropolyacids. *Catalysis Today*, *164*(1), 461–466. <https://doi.org/10.1016/j.cattod.2010.10.055>
- 21 Zou, X., Qin, T., Wang, Y., & Huang, L. (2011). Mechanisms and product specialties of the alcoholysis processes of poplar components. *Energy Fuels*, *25*(8), 3786–3792. <https://doi.org/10.1021/ef200726w>
- 22 Hishikawa, Y., Yamaguchi, M., Kubo, S., & Yamada, T. (2013). Direct preparation of butyl levulinate by a single solvolysis process of cellulose. *J. Wood Sci.*, *59*, 179–182. <https://doi.org/10.1007/s10086-013-1324-8>
- 23 Wang, Y., Yao, S., Jin, G., Qian, L., & Song, H. (2017). Catalytic alcoholysis of bagasse cellulose for the total reducing sugars with temperature-sensitive phase-variable ionic liquid. *Separation Science and Technology*, *52*(15), 2456–2462. <https://doi.org/10.1080/01496395.2017.1307225>
- 24 Chen, X., Zhang, Y., Mei, J., Zhao, G., Lyu, Q., Lyu, X., Lyu, H., Han, L., & Xiao, W. (2019). Ball milling for cellulose depolymerization and alcoholysis to produce methyl levulinate at mild temperature. *Fuel Process. Technol.*, *188*, 129–136. <https://doi.org/10.1016/j.fuproc.2019.02.002>
- 25 Chen, W., Zhang, Q., Lin, X., Jiang, K., & Han, D. (2020). The degradation and repolymerization analysis on solvolysis liquefaction of corn stalk. *Polymers*, *12*(10), 2337. <https://doi.org/10.3390/polym12102337>
- 26 Zhou, L., Gao, D., Yang, J., Yang, X., Su, Y., & Lu, T. (2020). Conversion of recalcitrant cellulose to alkyl levulinates and levulinic acid via oxidation pretreatment combined with alcoholysis over Al<sub>2</sub>(SO<sub>4</sub>)<sub>3</sub>. *Cellulose*, *2*(3), 1451–1463. <https://doi.org/10.1007/s10570-019-02903-1>
- 27 Badgujar, K. C., Badgujar, V. C., & Bhanage, B. M. (2023). Synthesis of alkyl levulinate as fuel blending agent by catalytic valorization of carbohydrates via alcoholysis: Recent advances and challenges. *Catal. Today*, *408*, 9–21. <https://doi.org/10.1016/j.cattod.2022.10.008>
- 28 Surov, O. V., Afineevskii, A. V., & Voronova, M. I. (2023). Sulfuric acid alcoholysis as a way to obtain cellulose nanocrystals. *Cellulose*, *30*, 9391–9404. <https://doi.org/10.1007/s10570-023-05470-8>
- 29 Lee, M., Heo, M., Lee, H., & Shin, J. (2021). Facile and quantitative method for estimating the isolation degree of cellulose nanocrystals (CNCs) suspensions. *Materials*, *14*(21), 6463. <https://doi.org/10.3390/ma14216463>
- 30 Beck, S., Bouchard, J., & Berry, R. (2012). Dispersibility in water of dried nanocrystalline cellulose. *Biomacromolecules*, *13*(5), 1486–1494. <https://doi.org/10.1021/bm300191k>
- 31 Segal, L., Creely, J. J., Martin, A. E., & Conrad, C. M. (1959). An empirical method for estimating the degree of crystallinity of native cellulose using the X-ray diffractometer. *Text. Res. J.*, *29*(10), 786–794. <https://doi.org/10.1177/004051755902901003>
- 32 Scherrer, P. (1918). Bestimmung der Größe und der inneren Struktur von Kolloidteilchen mittels Röntgenstrahlen. *Nachrichten von der Gesellschaft der Wissenschaften zu Göttingen, Mathematisch-physikalische Klasse*, *1918*, 98–100.

- 33 Rubleva, N. V., Lebedeva, E. O., Afineevskii, A. V., Voronova, M. I., Surov, O. V., & Zakharov, A. G. (2019). Production of cellulose nanocrystals by hydrolysis in mixture of hydrochloric and nitric acids. *ChemChemTech*, 62(12), 85–93. <https://doi.org/10.6060/ivkkt.20196212.5984>
- 34 Gaiolas, C., Belgacem, M. N., Silva, L., Thielemans, W., Costa, A. P., Nunes, M., & Silva, M. J. S. (2009). Green chemicals and process to graft cellulose fibers. *J. Colloid. Interface Sci.*, 330(2), 298–302. <https://doi.org/10.1016/j.jcis.2008.10.059>
- 35 Surov, O. V., Voronova, M. I., Rubleva, N. V., Kuzmicheva, L. A., Nikitin, D., Choukourov, A. Titov, V. A., & Zakharov, A. G. (2018). A novel effective approach of nanocrystalline cellulose production: Oxidation–hydrolysis strategy. *Cellulose*, 25, 5035–5048. <https://doi.org/10.1007/s10570-018-1910-4>
- 36 Voronova, M. I., Surov, O. V., & Zakharov, A. G. (2013). Nanocrystalline cellulose with various contents of sulfate groups. *Carbohydr. Polym.*, 98(1), 465–469. <https://doi.org/10.1016/j.carbpol.2013.06.004>
- 37 Voronova, M. I., Surov, O. V., Kuziyeva, M. K., & Atakhanov, A. A. (2022). Thermal and mechanical properties of polymer composites reinforced by sulfuric acid-hydrolyzed and TEMPO-oxidized nanocellulose: a comparative study. *ChemChemTech*, 65(10), 95–105. <https://doi.org/10.6060/ivkkt.20226510.6596>
- 38 Lin, N., & Dufresne, A. (2014). Surface chemistry, morphological analysis and properties of cellulose nanocrystals with gradiented sulfation degrees. *Nanoscale*, 6, 5384–5393. <https://doi.org/10.1039/C3NR06761K>
- 39 French, A. D. (2013). Idealized powder diffraction patterns for cellulose polymorphs. *Cellulose*, 21(2), 885–896. <https://doi.org/10.1007/s10570-013-0030-4>
- 40 Kontturi, E., Meriluoto, A., Penttila, P. A., Baccile, N., Malho, J. -M., Potthast, A., Rosenau, T., Ruokolainen, J., Serimaa, R., Laine, J., & Sixta, H. (2016). Degradation and crystallization of cellulose in hydrogen chloride vapor for high-yield isolation of cellulose nanocrystals. *Angew. Chem. Int. Ed.*, 55(46), 14455–14458. <https://doi.org/10.1002/anie.201606626>
- 41 Lorenz, M., Sattler, S., Reza, M., Bismarck, A., & Kontturi, E. (2017). Cellulose nanocrystals by acid vapour: towards more effortless isolation of cellulose nanocrystals. *Faraday Discuss.*, 202, 315–330. <https://doi.org/10.1039/C7FD00053G>
- 42 Adar, F. (2016). Characterizing modified celluloses using Raman spectroscopy. *Spectroscopy*, 31(11), 29–32. [www.spectroscopyonline.com](http://www.spectroscopyonline.com)
- 43 Makarem, M., Lee, C. M., Kafle, K., Huang, S., Chae, I., Yang, H., Kubicki, J. D., & Kim, S. H. (2019). Probing cellulose structures with vibrational spectroscopy. *Cellulose*, 26, 35–79. <https://doi.org/10.1007/s10570-018-2199-z>
- 44 Agarwal, U. P., Ralph, S. A., Baez, C., & Reiner, R. S. (2021). Detection and quantitation of cellulose II by Raman spectroscopy. *Cellulose*, 28, 9069–9079. <https://doi.org/10.1007/s10570-021-04124-x>
- 45 Agarwal, U. P. (2017). Raman spectroscopy in the analysis of cellulose nanomaterials. In U.P. Agarwal, R.H. Atalla, & A. Isogai (Eds.), *Nanocelluloses: Their preparation, properties, and applications* (ACS Symposium Series, 1251, 4, 75–90). <https://doi.org/10.1021/bk-2017-1251.ch004>
- 46 Agarwal, U. P., Ralph, S. A., Reiner, R. S., & Baez, C. (2018). New cellulose crystallinity estimation method that differentiates between organized and crystalline phases. *Carbohydr. Polym.*, 190, 262–270. <https://doi.org/10.1016/j.carbpol.2018.03.003>
- 47 Zhang, K., Brendler, E., & Fischer, S. (2010). FT Raman investigation of sodium cellulose sulfate. *Cellulose*, 17, 427–435. <https://doi.org/10.1007/s10570-009-9375-0>
- 48 Agarwal, U. P., Reiner, R. S., Ralph, S. A., Catchmark, J., Chi, K., Foster, E. J., Hunt, C. G., Baez, C., Ibach, R. E., & Hirth, K. C. (2021). Characterization of the supramolecular structures of cellulose nanocrystals of different origins. *Cellulose*, 28, 1369–1385. <https://doi.org/10.1007/s10570-020-03590-z>
- 49 Li, Q., & Renneckar, S. (2011). Supramolecular structure characterization of molecularly thin cellulose I nanoparticles. *Biomacromolecules*, 12, 650–659. <https://doi.org/10.1021/bm101315y>
- 50 Agarwal, U. P., Ralph, S. A., Reiner, R. S., & Baez, C. (2016). Probing crystallinity of never-dried wood cellulose with Raman spectroscopy. *Cellulose*, 23, 125–144. <https://doi.org/10.1007/s10570-015-0788-7>
- 51 Reutov, O. A., Kurts, A. L., & Butin, K. P. (2021). *Organicheskaya khimiya [Organic chemistry]*. Laboratoriia znaniia [in Russian].
- 52 Bruice, P. Y. (2009). *Essential organic chemistry* (2nd ed.). Prentice Hall.
- 53 Ripin, D. H. B. (2011). pKa. In S. Caron (Ed.), *Practical synthetic organic chemistry: Reactions, principles, and techniques* (1st ed., chapter 18, pp. 771–803). Wiley. <https://doi.org/10.1002/9781118093559.ch18>
- 54 El Seoud, O. A., Fidale, L. C., Ruiz, N., D’Almeida, M. L. O., & Frollini, E. (2008). Cellulose swelling by protic solvents: which properties of the biopolymer and the solvent matter? *Cellulose*, 15, 371–392. <https://doi.org/10.1007/s10570-007-9189-x>
- 55 Zhao, H., Jia, Y., Liang, X., Hao, J., Xu, G., Chen, B., He, C., Jiao, Y., & Chang, C. (2024). Theoretical and experimental study of 5-ethoxymethylfurfural and ethyl levulinate production from cellulose. *Chem. Eng. J.*, 480, 148093. <https://doi.org/10.1016/j.cej.2023.148093>